Dalton Transactions

ROYAL SOCIETY OF CHEMISTRY

PAPER

View Article Online
View Journal | View Issue



Cite this: *Dalton Trans.*, 2024, **53**, 10453

# Conductance and assembly of quasi-1D coordination chain molecular junctions with triazole derivatives†

Zelin Miao,[a] Xiaoyun Pan[b] and Maria Kamenetska *[a,b,c]

Incorporating transition metal atoms into metal–molecule–metal junctions presents opportunities for exploring the electronic properties of coordination complexes, organometallics and metal–organic materials on the single molecule level. Recent single molecule conductance studies have shown that *in situ* incorporation of electrode metal atoms into coordination chains formed in the junction can occur with deprotonated, negatively charged organic ligands, such as the imidazolate ($Im^-$) anion. However, the mechanism and chemical principles, such as the role of the charge state of the ligand, for the construction of such coordination chains are still debated. Here, we probe the role of the ligand charge state and electronic structure in single-molecule conductance and formation of metal–molecule coordination chains. We perform break junction measurements with triazole isomers, which can bridge junctions both in their neutral and charged forms, and find that prior deprotonation of the ligands is not required for coordination complex assembly, but can affect the molecular conductance and junction formation probability. Our results indicate that coordination chains can form with neutral ligands, as long as the electron density in the frontier MOs is concentrated at the binding sites and along the direction of pulling, promoting ligand binding and incorporation of gold atoms into the junction during elongation. Our findings may provide insight into design principles for *in situ* assembled molecular wires with transition metal atoms and open the door to electronic and spintronic studies of such materials.

Received 13th April 2024,
Accepted 10th June 2024

DOI: 10.1039/d4dt01085j

rsc.li/dalton



Incorporating transition metal atoms into molecular junctions has the potential to expand the scope of phenomena in nanoscale devices due to increased spin and orbital degrees of freedom.[1,2] Prior studies suggest that metal atom-containing junctions can serve as qubits,[3–5] switches,[6–9] spin valves,[10–12] and other memory and spintronic devices.[13–15] However, significant challenges to incorporating molecules with metal cores persist. We and others have recently shown that the donor–acceptor intramolecular interactions that characterize many inorganic coordination complexes are sometimes incompatible with the junction environment and lead to distortion and disassembly of the *ex situ* synthesized complexes on electrode surfaces.[16–19]

An alternative avenue towards assembly of the metal-atom containing junctions is *in situ* organometallic or coordination chain formation from organic precursors. We and others have demonstrated that extraction of gold atoms from the electrode and into the molecular wire can occur with certain ligands during junction elongation.[20–22] For example, our previous study of imidazole (Im), depicted in Fig. 1a, shows that this heterocyclic compound with two non-adjacent nitrogen atoms (N1 and N3), once deprotonated to imidazolate ($Im^-$), can bridge source–drain nanogaps through dative interaction between nitrogen and undercoordinated gold surface sites to form molecular junctions.[22–25] Upon further tip retraction, longer chains composed of $Im^-$–Au–$Im^-$ are generated, as schematically illustrated in Fig. 1b. Other molecular systems, including isocyano-terminated benzenes[20] and the unprotected terminal alkynes,[21,26] exhibit similar behavior, suggesting that this bottom-up strategy is a promising direction for achieving such functional metal-containing molecular devices.

In most prior work, the precursor ligands are organic anions, suggesting that charged species are required for assembly to occur. For example, our published results showed that the presence of the negative charge on the $Im^-$ molecule

[a]*Division of Materials Science and Engineering, Boston University, Boston, Massachusetts, 02215, USA. E-mail: mkamenet@bu.edu*
[b]*Department of Chemistry, Boston University, Boston, Massachusetts, 02215, USA*
[c]*Department of Physics, Boston University, Boston, Massachusetts, 02215, USA*

†Electronic supplementary information (ESI) available: STM-BJ procedure, sample-preparation, error analysis and computational details, conductance measurements of Tr123 with varying pH, bias-dependent controls, MOs of triazole isomers, eigenchannel analysis, binding energy and additional transmission spectra of junctions. See DOI: https://doi.org/10.1039/d4dt01085j

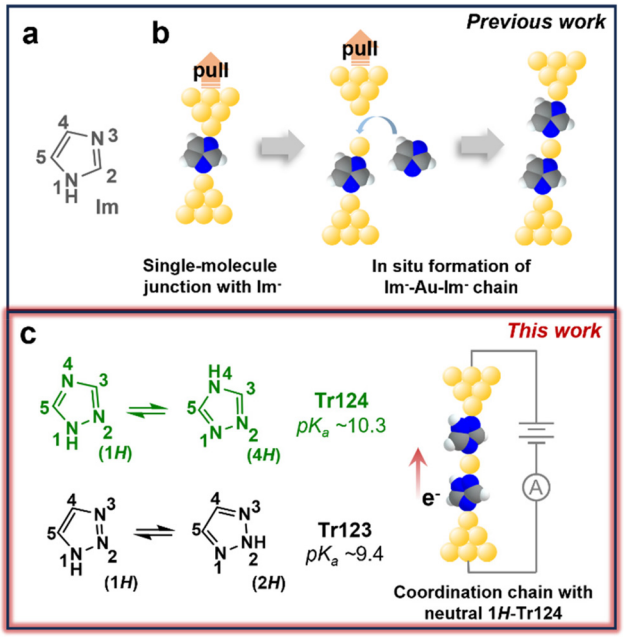


**Fig. 1** (a) Chemical structure of imidazole (Im) investigated in previous work.[22] (b) Schematic illustration of a single $Im^-$ molecule bound between gold electrodes and the *in situ* metal–molecule chain formation with $Im^-$ upon junction elongation. (c) Chemical structures and tautomeric isomerization of 1,2,4-triazole (Tr124) and 1,2,3-triazole (Tr123) in aqueous solutions. The $pK_a$ values of Tr124 and Tr123 are ~10.3 and ~9.4, respectively.[37] We show in this work that coordination chains can also be constructed with neutral Tr123 and Tr124. Color code: N, blue; C, gray; H, white; Au, yellow.

could strengthen the Au–N bond and allow for the disruption of the gold electrode and the incorporation of gold atoms into the junction.[22] Yet the exact molecular mechanism of chain formation remains unclear.[27]

Here, we examine the chemical requirements for the *in situ* coordination chain assembly by studying the conductance and junction formation with imidazole variants—triazoles. The molecular structures of two triazole isomers, 1,2,4-triazole (Tr124) and 1,2,3-triazole (Tr123), are shown in Fig. 1c. These isomers and their derivatives are commonly used organic ligands for applications requiring robust binding to transition metals through the electron lone pairs on the nitrogens, such as for the synthesis of coordination compounds with significant spin-crossover properties,[28,29] or as corrosion inhibitors to passivate metal surfaces (*e.g.*, copper and steel) in extreme conditions.[30,31] Here, we use them to bridge gold electrodes to form molecular junctions. Both triazole scaffolds contain three potential gold-binding sites—one pyrrole nitrogen (–NH–) and two tertiary amines (=N–, pyridine-like nitrogen atoms).[22,32,33] When dissolved in water, each isomer exists as a pair of tautomers accessed by intermolecular double-proton transfer with low activation barriers,[34–36] as indicated by tautomeric equilibriums shown in the schemes (Fig. 1c). The tautomeric isomerization of neutral molecules exposes two binding groups either at adjacent (4*H*-Tr124 and 1*H*-Tr123) or non-adjacent (1*H*-Tr124 and 2*H*-Tr123) positions. In basic conditions, when the pyrrole nitrogen is deprotonated to form triazolide anions ($Tr124^-$ and $Tr123^-$), an additional nitrogen anchor site to gold is exposed.

By measuring the conductance and 1D molecular chain assembly with triazoles in different solvent environments, we establish the transport characteristics of triazole-based molecular junctions in the neutral and anionic states. Specifically, our experimental results show that both triazole isomers in the neutral state can form single-molecule junctions and assemble into molecular chains, suggesting that ionic charge is not essential for chain formation. Furthermore, deprotonation facilitates electron transport and chain formation probability of Tr123 but lowers the conductance and broadens the signatures of Tr124. By comparing these experimental observations with DFT calculations, we are able to infer which molecular orbital features contribute to successful chain formation. We find that the structure of the frontier molecular orbitals (MOs) and the availability of the lone pairs on non-adjacent nitrogens for binding are the decisive factors in the probability of *in situ* chain assembly. Our work here may help uncover and establish the chemical requirements for incorporating transition metal atoms into quasi-1D molecular wires in the junctions.

We perform single-molecule conductance measurements using a home-built scanning tunneling microscope break-junction (STM-BJ) instrument following established protocols, as previously described (see ESI† for more details).[38,39] In a typical experiment, we repeatedly smash in and pull apart two gold electrodes with sub-angstrom precision to form source–drain nanogaps under a constant bias. These gaps can be bridged by molecules that self-assemble between the gold electrodes through electron donor sites on the molecule. Conductance (current/voltage) is measured as a function of the relative displacement of electrodes during junction elongation at a bias of 100 mV or 500 mV. Thousands of such measurements are recorded and compiled into conductance histograms which are fit to Gaussian curves to extract the most probable conductance values. We measure the two triazole isomers from Fig. 1c and their methylated derivatives discussed further below in organic solvents, *N*,*N*-dimethylformamide (DMF) and 1,2,4-tricholorobenzene (TCB), or dip-coated onto the substrates out of aqueous solutions as described in the ESI† and in our previous work.[22,40,41] Measurements in aqueous liquid conditions using the wax-coated tip are also performed and shown in the ESI† for comparison to the dip-coated measurements. Both dried and aqueous conditions yield the same molecular conductance values, but the signal-to-noise is higher in dried dip-coated samples (Fig. S1†).[22] Therefore, all measurements shown in the manuscript are performed in dry conditions except those in organic solvents.

We first measure the conductance of Tr124 and Tr123 in DMF solutions, where the neutral motifs of triazoles are predominant, using wax-coated tips to suppress the ionic background current.[42] The histograms for both molecules, shown

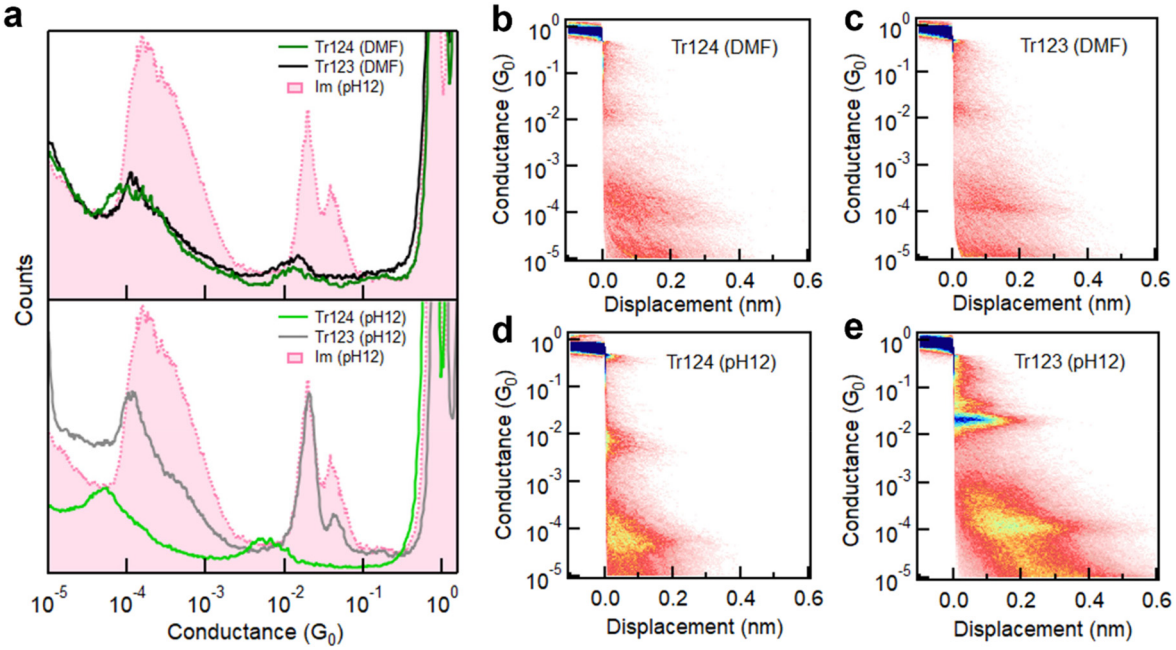


**Fig. 2** (a) Top: overlaid 1D log-binned conductance histograms of Tr124 (green) and Tr123 (black) measured in DMF solutions using the wax-coated tips to provide ionic isolation. Bottom: conductance histograms of $Tr124^-$ and $Tr123^-$ dip-coated on gold samples from pH 12 aqueous solutions. Conductance histogram of $Im^-$ is plotted for comparison.[22] All histograms are constructed from at least 4000 consecutive individual traces without any data selection. (b and c) 2D conductance-displacement histograms compiled from thousands of traces of Tr123 and Tr124 in DMF solutions or (d and e) of $Tr123^-$ and Tr $124^-$ dip-coated from water at pH 12.

in Fig. 2a (top panel), are compiled from 4000 consecutive measured traces without any data selection. We observe similar conductance features for both isomers within two distinct regimes at $\sim 10^{-2}$ $G_0$ (high-G) and $\sim 10^{-4}$ $G_0$ (low-G). Compared to our previous work on $Im^-$ replotted here in pink, this suggests that the high-G peaks result from one or several molecules bound in parallel, similar to $Im^-$ (Fig. 1b, left), while the low-G features are due to chain formation where the molecules are bound in series (Fig. 1b and c, right).[22,41] Notably, the extension lengths that junctions can sustain for both isomers in low-G are ~4 Å, approximately double that of high-G plateaus, as shown in 2D conductance-displacement histograms (Fig. 2b and c). The presence of both the high- and low-G features in triazole data, their similarity to $Im^-$ signatures, and the relative extensions indicate that neutral triazoles in DMF can bind to gold through opposite tertiary amines present in both isomers (N2/N4 in 1*H*-Tr124 and N1/N3 in 2*H*-Tr123 as shown in Fig. 1c), analogously to the geometry of $Im^-$ junctions.[22,25]

The most probable high-G conductance values for Tr124 and Tr123 are $1.27 \times 10^{-2}$ $G_0$ and $1.31 \times 10^{-2}$ $G_0$, respectively, which are ~35% lower than the conductance of $Im^-$. We note that the amplitude of the conductance peaks with neutral triazoles is also lower than with $Im^-$ measured in dried condition, for both high-G and low-G signatures. This feature may be due to the different environments in which the measurements were performed which we explore below. Nevertheless, these results collectively suggest that neutral triazole motifs, whether Tr124 or Tr123, can form extended metal–molecule chains in DMF and that anionic character is not required for *in situ* coordination complex assembly.

To test if the deprotonation of triazoles can affect their junction binding and transport characteristics, we perform break-junction measurements of Tr123 and Tr124 by depositing molecules from aqueous pH 12 solutions on gold. In such basic environments, where pH ≥ p$K_a$ (Fig. 1c), the equilibrium of both triazole molecules shifts towards the anionic states. The resulting conductance histograms compiled out of 5000 individual traces are plotted in the bottom panel of Fig. 2a. In these conditions, the conductance characteristics of the two triazole anions are distinct. In both cases, we still observe high-G and low-G conductance signatures. Consulting 2D histograms of both isomers in Fig. 2d–e we note that the low-G plateaus persist on average twice as long as high-G features, similar to their neutral analogs. However, with $Tr123^-$, the high-G value corresponding to the single molecule junction (highest amplitude peak) is found to be $2.01 \times 10^{-2}$ $G_0$, which is in good agreement with the conductance of $Im^-$. This correspondence reveals that once it becomes deprotonated, $Tr123^-$ is likely to adopt a similar binding configuration as $Im^-$ anchoring to gold through non-adjacent nitrogen atoms at N1 and N3 positions, while the N2 nitrogen in between has negligible impact on conductance or binding. Chain formation probability is also robust, as indicated by the high peak amplitude. In contrast, for anionic $Tr124^-$, a broad peak with conductance of $5.39 \times 10^{-3}$ $G_0$ (measured at 100 mV) occurs in the

high-G region, which is significantly lower than the single molecule conductance of $Tr123^-$ and $Im^-$. The conductance of the chain is similarly lower than in $Tr123^-$ or in $Im^-$. We also note that $Tr124^-$ displays a lower chain formation yield as indicated by the decreased amplitude of its low-G feature compared to $Tr123^-$.

We supplement the conductance measurement of Tr124 in pH 12 shown above with measurements in pH 1.5, 3, and 9 in Fig. 3a (see Fig. S2† for measurements of Tr123 at varying pH conditions). These pH conditions are selected to probe the distinct charged states of Tr124, which is characterized by two $pK_a$ values;[37] at pH < 2.2, the molecule is a triazolium cation $Tr124^+$; at pH > 10.3, it becomes deprotonated to triazolide anion $Tr124^-$. We observe distinct signatures in each pH regime. At pH 1.5, there is a single broad peak at $\sim10^{-3}$ $G_0$. This feature has been previously attributed to through-space transport associated with the π–π stacks of two molecules bound on opposite electrodes.[22,43] These measurements are consistent with $Tr124^+$, which only has one unprotonated binding site. At pH 3, through-space transport is still present. However, the high-G and low-G bridging features start appearing at $\sim10^{-2}$ and $10^{-4}$ $G_0$ due to an equilibrium between triazolium cation and neutral triazole in this condition. At pH 9, π–π stacking features are gone, and the conductance resembles signatures of the neutral Tr124 molecule that we measured in DMF in Fig. 2a (replotted in Fig. 3b). We list the average single-molecule conductance (high-G) data in Table 1 and note that the high-G conductance values of Tr124 in DMF and at pH = 9 are within experimental error (see ESI† for more details). Notably, the conductance and amplitude of the broad high-G feature appearing at pH 12 (with applied bias of 500 mV) are distinct and lower than at pH 9. Based on these results, we conclude that the junction formation probability for the anionic $Tr124^-$ is lower than for neutral analog deposited from the aqueous environments. Control measurements of triazole isomers at each pH condition at different biases show no significant bias dependence for both high-G and low-G signatures (Fig. S3 and S4†).

To rule out the possibility of junction bridging of Tr124 through two adjacent nitrogen atoms, we measure the conductance of two Tr124 derivatives: 4-methyl-4*H*-1,2,4-triazole (4Me-Tr124) and 1-methyl-1,2,4-triazole (1Me-Tr124) in TCB (Fig. 3b, see 2D conductance histogram in Fig. S5†). In these molecules, non-exchangeable methyl groups substitute the hydrogen atom[44] to block one of the nitrogen sites from binding with gold. We observe only a broad π–π stacking conductance signature at $\sim10^{-3}$ $G_0$ for 4Me-Tr124 in which only adjacent nitrogen binding sites are present, confirming that bridging the junction through adjacent nitrogen sites is unlikely. For 1Me-Tr124, the peak at $\sim10^{-2}$ $G_0$ is broadly consistent with neutral Tr124 measured in DMF and pH 9 aqueous solutions, with a slight shift to the lower value due to the methyl substituent.[45] These results further confirm that neutral Tr124 is responsible for the high-G single-molecule feature, as summarized in Table 1. Notably, the low-G conductance peak is also present with 1Me-Tr124 in this non-aqueous organic solvent, confirming that chain formation with neutral Tr124 analogs can occur. To summarize, our data suggest that we capture distinct charge states of Tr124 at different pH environments, and, more importantly, that the binding to gold electrodes through two tertiary amine nitrogens in neutral Tr124 can lead to more robust and higher conducting single-molecule junctions and low-G chains in comparison to its anionic analog (see the ESI† for the discussion regarding Tr123).

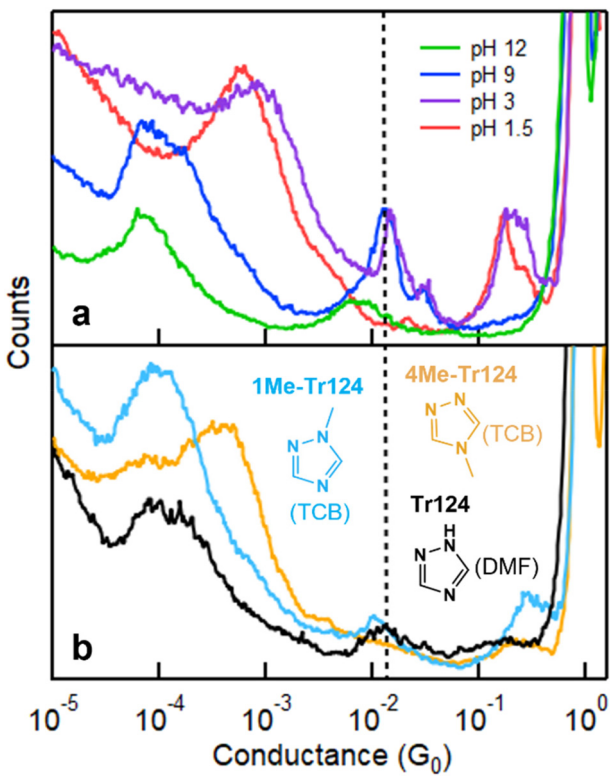


**Fig. 3** (a) Conductance measurements of Tr124 through molecular deposition out of aqueous solutions with varying pH values under bias of 500 mV. Dissolving molecules in neutral $H_2O$ results in solution with pH ~ 9. Each histogram is constructed from 5000 individual traces. (b) Conductance histograms of control molecules including 1-methyl-1,2,4-triazole (1Me-Tr124) and 4-methyl-4*H*-1,2,4-triazole (4Me-Tr124) measured in TCB solutions. Histogram for Tr124 measured in DMF from Fig. 2a is reproduced here for convenience.

**Table 1** The most probable conductance values of high-G peaks ($\sim10^{-2}$ $G_0$) of triazole derivatives with different solvents and pH conditions

| | Solvent | pH | Conductance (experimental, $G_0$) |
|---|---|---|---|
| Im | $H_2O$ | 12 | $1.96 \times 10^{-2}$ |
| Tr124 | $H_2O$ | 12 | $7.03 \times 10^{-3}$ |
| | $H_2O$ | 9 | $1.29 \times 10^{-2}$ |
| | DMF | N/A | $1.27 \times 10^{-2}$ |
| 1Me-Tr124 | TCB | N/A | $1.05 \times 10^{-2}$ |
| Tr123 | $H_2O$ | 12 | $2.01 \times 10^{-2}$ |
| | $H_2O$ | 8 | $1.94 \times 10^{-2}$ |
| | DMF | N/A | $1.31 \times 10^{-2}$ |

We turn to first-principles density functional theory (DFT) calculations to provide insights into the origin of different conductance trends and coordination chain formation with neutral and anionic Tr124 and Tr123 discussed above. FHI-aims package equipped with the AITRANSS module[46–48] and Perdew–Burke–Ernzerhof (PBE) density functional[49] is applied to calculate junction geometries, gas-phase molecular orbitals (MOs), and electron transport through the molecular junctions using previously established protocols[50] with details provided in the ESI.† The relaxed junction structures and transmission spectra for neutral and anionic systems are shown in Fig. 4a and b, respectively. In all cases, the most stable junction structures are formed with molecules bound through non-adjacent nitrogen atoms in agreement with experimental measurements. The binding energy of neutral N–Au bonds is characteristic of pyridine–gold type interactions at 0.4–0.5 eV, but the binding of the anionic species is ~1.5–2 eV (see ESI† for more details of binding energy calculations).[25,56] These results are consistent with our prior findings for the $Im^-$ junction system.

The predicted transmission spectra of neutral Tr123 and Tr124 are shown in Fig. 4a. We observe that the LUMO resonances are closer to $E_F$ for these neutral motifs, suggesting that LUMO dominates transport at low bias for both molecules. The transmission at Fermi, indicated by a dashed line, is nearly identical for both molecules, consistent with the measured conductance of Tr123 and Tr124 in DMF solutions shown in Fig. 2a.

In contrast, we find that the transport of anionic Tr124 and Tr123 junctions are HOMO-dominated because the transmission peaks at ~−1.7 eV are closer to and have more overlap with $E_F$ than the LUMO peaks at ~3.5 eV (Fig. 4b). Calculated transmission values of $Tr123^-$ and $Tr124^-$ are $5.47 \times 10^{-2}$ $G_0$ and $4.45 \times 10^{-2}$ $G_0$, respectively. The difference is in qualitative agreement with our experimental observations that $Tr123^-$ has higher conductance than $Tr124^-$ (Fig. 2a). We note the general overestimation of DFT-based transport calculation compared to the measured conductance for single-molecule junctions is

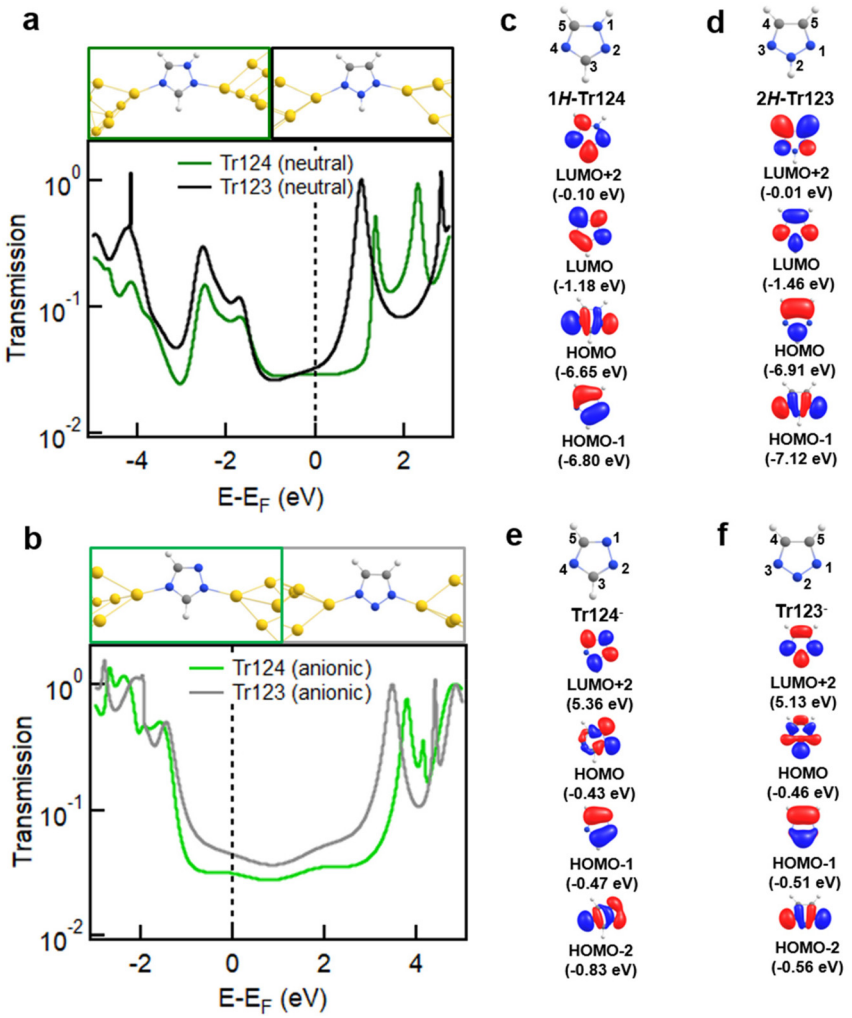


**Fig. 4** (a, b) Relaxed junction geometries with neutral and anionic Tr124 and Tr123 bound between two Au18 pyramids with the apex Au–Au distance corresponding to potential energy minimum (top) and the calculated transmission spectra (bottom). Frontier MOs of Tr124 and Tr123 in neutral (c, d) and anionic (e, f) forms and calculated using FHI-aims package with a "tight" basis set and the PBE functional (see Fig. S6 and S7† for the complete pictures of MO plotting).

consistent with the disparity reported in previous studies.[51–55] We conclude that the differences in the energy alignment and reduced coupling of HOMO with $E_F$ in the anionic triazoles are partially responsible for the lower conductance of the $Tr124^-$ compared to $Tr123^-$.

Frontier MOs of neutral and anionic Tr124 and Tr123 isomers relevant for junction binding and transport are depicted in Fig. 4c, d and e, f, respectively. We observe σ character on both non-adjacent nitrogen atoms in HOMO or HOMO−1 (for 2*H*-Tr123) in all four species. The complete set of gas-phase MOs of all the triazole isomers are shown in Fig. S6 and S7.† This result is consistent with prior studies showing that pyridine nitrogen binds to gold through the electron lone pairs in the σ framework, which is part of the filled states even if the main transmission channel is dominated by the molecular LUMO.[25,56] Specifically, in the neutral analogs, the high electron density at the non-adjacent nitrogens is concentrated in the σ-dominated and closely spaced HOMO and HOMO−1, indicating the availability of electron lone-pairs on those sites to bind to gold. The role of HOMO σ orbitals in junction binding is also evident in the eigenchannel analysis of neutral Tr123 and Tr124 shown in Fig. S8 and S9,† respectively. We observe high electron density at the N–Au bonds in the filled part of the spectrum and note that it is aligned with the junction elongation direction. The π-LUMO orbitals which dominate transport are similar in their distribution across the two neutral molecules. Overall, this analysis is consistent with experimentally determined similarity in junction yield and conductance values of neutral triazoles.

Turning to the anionic species, we note that the high electron density at the lone pair sites is also present in $Tr123^-$ on the closely spaced σ HOMO and HOMO−2. Similar to neutral triazoles, the resulting N–Au bond exhibits high electron density and aligns with the pulling direction, as illustrated in Fig. S10.† In contrast, in $Tr124^-$ gas-phase HOMO−2 is further below the HOMO, indicating a reduced ability of this MO to transfer charge to the gold during binding. The remaining HOMO orbital has a node, or no charge density, on the N4, as shown in Fig. 4e, and is instead concentrated on the adjacent N1 and N2 nitrogen atoms. This change is reflected in the junction eigenchannel analysis for $Tr124^-$ in Fig. S11,† where less electron density is observed in the N–Au bond on $Tr124^-$, particularly in the HOMO resonance. The concentration of charge on the adjacent nitrogen atoms increases the likelihood of $Tr124^-$ binding to one electrode with both N1 and N2, as shown in Fig. S12.†[32] This geometry has a reduced binding energy between N4 and gold and may explain the shorter plateaus and the lower likelihood of chain assembly observed with $Tr124^-$. In Fig. S13,† we show that the transmission through such junctions where all three nitrogen atoms are bound to electrodes (which is only likely with $Tr124^-$) is quite distinct from the two-nitrogen bridging geometry and will broaden the conductance distribution observed with this molecule. Overall, the low density of the σ-MOs on the N4 and the large number of available geometries associated with $Tr124^-$ likely account for the broadness and low amplitude of its high-G conductance peak compared to its neutral analogues and to $Tr123^-$.

DFT transport calculations of the extended chains formed with anionic Tr123 and Tr124 are also shown in Fig. 5 (the spectra of the corresponding neutral analogs are displayed in Fig. S14†). We note that in terms of the chain configurations as well, $Tr124^-$ has numerous binding orientations with respect to the direction of the adjacent nitrogen atoms (dashed arrows in Fig. 5, top), while $Tr123^-$ only has one symmetric geometry. Transport calculations in Fig. 5 (bottom) show that transmission through the distinct junctions of $Tr124^-$ chains varies at the Fermi energy, which is in qualitatively agreement with the broadened conductance distribution we observe in experiments. Chain configurations where both N1 and N2 bind to one electrode as in Fig. S13† or to both electrodes (not shown) are also possible and may further broaden the conductance distribution measured with the $Tr124^-$ chains. The predicted conductance of the $Tr123^-$ chain is $1.96 \times 10^{-4}\ G_0$, which is higher than the predicted average of the $Tr124^-$ chains at $7.95 \times 10^{-5}\ G_0$, consistent with our experimental results. Overall, we conclude that the asymmetry of $Tr124^-$ and the associated asymmetric MOs with reduced density on the N4 result in numerous binding orientations of this molecule in the junction, which interferes in the formation of a well-defined single molecule coordination wire and contributes to a broad conductance distribution observed in experiment.

In conclusion, we evaluate the effect of the molecular charge states of triazole isomers on the transport properties of single molecule–metal junctions and on the chain structure formation. We demonstrate identical conductance signatures of Tr123 and Tr124 in their neutral motifs and the evidence of quasi-1D chain formation in both molecules even in the absence of overall linker charge. In contrast, upon deprotonation, anionic $Tr124^-$ displays significant conductance suppression and a broadened conductance signature in comparison to $Tr123^-$. DFT calculations corroborate our experimental observations and suggest that deficient electron density on non-adjacent pyridine-like nitrogen atoms of $Tr124^-$ in gas-phase MOs results in a less favorable bridging of the junction electrodes, hampering the quasi-1D chain formation. Instead, $Tr124^-$ is more likely to bind to a single electrode with two adjacent tertiary amine nitrogens, resulting in various geometries all with distinct conductance values which broaden and wash out the molecular signature. Numerous configurations of $Tr124^-$ are also possible in the chain configuration, where the conductance is similarly broadened. Overall, our work reveals that anionic character is not required for *in situ* assembly of coordination chains but that controlling the electron density distribution within the molecule is key to engineering effective linkers for chain formation. Our work also emphasizes the particular importance of the σ network for coordination complex assembly in the junction. It suggests that good alignment between the binding MOs and the direction of junction elongation is a prerequisite for incorporating gold atoms from the electrode into the junction. Taken together, this work pro-

 

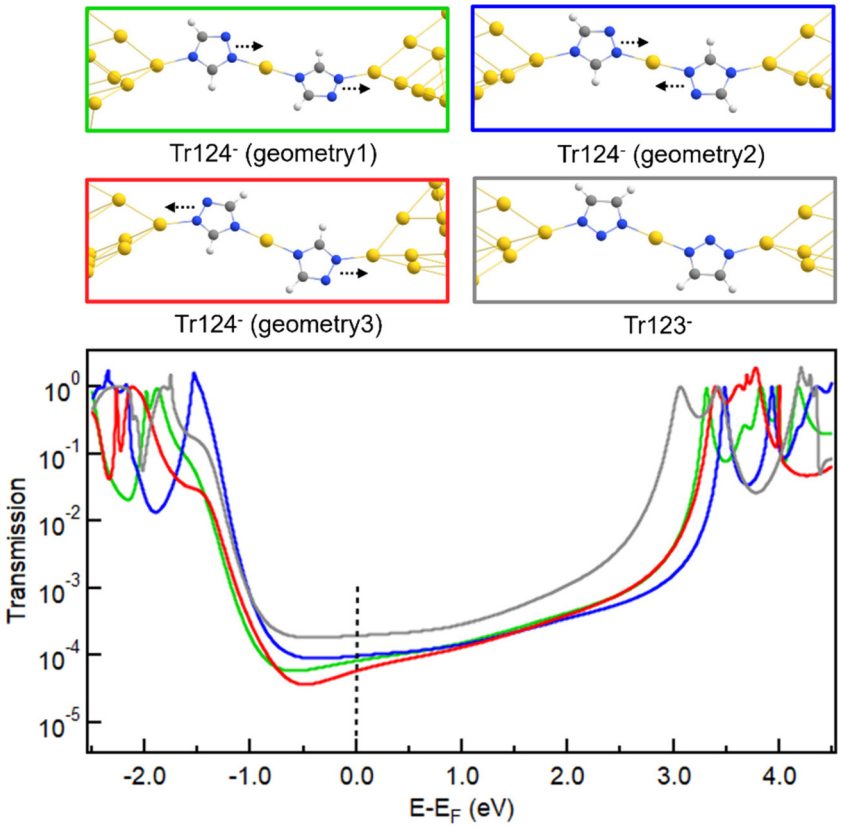


**Fig. 5** Junction structures with coordination chains comprising anionic Tr123$^{-}$ and accessible geometries of Tr124$^{-}$ with distinct arrangements of the two adjacent tertiary amines (=N–) with respect to the electrodes (indicated by the dashed arrows, top) and the corresponding transmission spectra (bottom). Configurations with one or both Tr124$^{-}$ molecule bound to dull gold electrodes through two adjacent nitrogens are also possible but are not included here. The number of electrons in the structure was adjusted to make the overall junction closed shell.

vides insight into chemical strategies for modulating single-molecule conductance and coordination chain assembly *via* electronic structure tuning.

## Data availability

All data can be made available upon reasonable request. We are not able to locate it in a public database due to data size considerations.

## Conflicts of interest

The authors declare no competing financial interest.

## Acknowledgements

This work was supported by the National Science Foundation under award #2145276. Z. M. acknowledges support from a BUnano Cross-Disciplinary Fellowship. All authors appreciate support from the BU Photonics Center where the work was performed. The authors gratefully thank Dr Brent Lawson and Sigifredo Luna for the useful discussions on DFT calculations.

## References

1 L. Bogani and W. Wernsdorfer, Molecular Spintronics Using Single-Molecule Magnets, *Nat. Mater.*, 2008, **7**, 179–186.
2 R. Vincent, S. Klyatskaya, M. Ruben, W. Wernsdorfer and F. Balestro, Electronic Read-out of a Single Nuclear Spin Using a Molecular Spin Transistor, *Nature*, 2012, **488**, 357–360.
3 A. Gaita-Ariño, F. Luis, S. Hill and E. Coronado, Molecular Spins for Quantum Computation, *Nat. Chem.*, 2019, **11**, 301–309.
4 S. Thiele, F. Balestro, R. Ballou, S. Klyatskaya, M. Ruben and W. Wernsdorfer, Electrically Driven Nuclear Spin Resonance in Single-Molecule Magnets, *Science*, 2014, **344**, 1135–1138.
5 A. A. Fursina and A. Sinitskii, Toward Molecular Spin Qubit Devices: Integration of Magnetic Molecules into Solid-State Devices, *ACS Appl. Electron. Mater.*, 2023, **5**, 3531–3545.

6 A. C. Aragonès, D. Aravena, J. I. Cerdá, Z. Acís-Castillo, H. Li, J. A. Real, F. Sanz, J. Hihath, E. Ruiz and I. Díez-Pérez, Large Conductance Switching in a Single-Molecule Device through Room Temperature Spin-Dependent Transport, *Nano Lett.*, 2016, **16**, 218–226.

7 S. Wagner, F. Kisslinger, S. Ballmann, F. Schramm, R. Chandrasekar, T. Bodenstein, O. Fuhr, D. Secker, K. Fink, M. Ruben and H. B. Weber, Switching of a Coupled Spin Pair in a Single-Molecule Junction, *Nat. Nanotechnol.*, 2013, **8**, 575–579.

8 M. Ormaza, P. Abufager, B. Verlhac, N. Bachellier, M. L. Bocquet, N. Lorente and L. Limot, Controlled Spin Switching in a Metallocene Molecular Junction, *Nat. Commun.*, 2017, **8**, 1974.

9 F. Schwarz, G. Kastlunger, F. Lissel, C. Egler-Lucas, S. N. Semenov, K. Venkatesan, H. Berke, R. Stadler and E. Lörtscher, Field-Induced Conductance Switching by Charge-State Alternation in Organometallic Single-Molecule Junctions, *Nat. Nanotechnol.*, 2016, **11**, 170–176.

10 A. N. Pal, D. Li, S. Sarkar, S. Chakrabarti, A. Vilan, L. Kronik, A. Smogunov and O. Tal, Nonmagnetic Single-Molecule Spin-Filter Based on Quantum Interference, *Nat. Commun.*, 2019, **10**, 5565.

11 M. Urdampilleta, S. Klyatskaya, J.-P. Cleuziou, M. Ruben and W. Wernsdorfer, Supramolecular Spin Valves, *Nat. Mater.*, 2011, **10**, 502–506.

12 A. K. Singh, S. Chakrabarti, A. Vilan, A. Smogunov and O. Tal, Electrically Controlled Bimetallic Junctions for Atomic-Scale Electronics, *Nano Lett.*, 2023, **23**, 7775–7781.

13 C. Timm and F. Elste, Spin Amplification, Reading, and Writing in Transport through Anisotropic Magnetic Molecules, *Phys. Rev. B: Condens. Matter Mater. Phys.*, 2006, **73**, 235304.

14 S. Schmaus, A. Bagrets, Y. Nahas, T. K. Yamada, A. Bork, M. Bowen, E. Beaurepaire, F. Evers and W. Wulfhekel, Giant Magnetoresistance through a Single Molecule, *Nat. Nanotechnol.*, 2011, **6**, 185–189.

15 S. L. Bayliss, D. W. Laorenza, P. J. Mintun, B. D. Kovos, D. E. Freedman and D. D. Awschalom, Optically Addressable Molecular Spins for Quantum Information Processing, *Science*, 2020, **370**, 1309–1312.

16 H. E. Skipper, C. V. May, A. L. Rheingold, L. H. Doerrer and M. Kamenetska, Hard-Soft Chemistry Design Principles for Predictive Assembly of Single Molecule-Metal Junctions, *J. Am. Chem. Soc.*, 2021, **143**, 16439–16447.

17 T. Knaak, C. González, Y. J. Dappe, G. D. Harzmann, T. Brandl, M. Mayor, R. Berndt and M. Gruber, Fragmentation and Distortion of Terpyridine-Based Spin-Crossover Complexes on Au(111), *J. Phys. Chem. C*, 2019, **123**, 4178–4185.

18 S. Rohlf, J. Grunwald, T. Jasper-Toennies, S. Johannsen, F. Diekmann, M. Studniarek, R. Berndt, F. Tuczek, K. Rossnagel and M. Gruber, Influence of Substrate Electronic Properties on the Integrity and Functionality of an Adsorbed Fe(II) Spin-Crossover Compound, *J. Phys. Chem. C*, 2019, **123**, 17774–17780.

19 S. Ossinger, H. Naggert, L. Kipgen, T. Jasper-Toennies, A. Rai, J. Rudnik, F. Nickel, L. M. Arruda, M. Bernien, W. Kuch, R. Berndt and F. Tuczek, Vacuum-Evaporable Spin-Crossover Complexes in Direct Contact with a Solid Surface: Bismuth versus Gold, *J. Phys. Chem. C*, 2017, **121**(2), 1210–1219.

20 A. Vladyka, M. L. Perrin, J. Overbeck, R. R. Ferradás, V. García-Suárez, M. Gantenbein, J. Brunner, M. Mayor, J. Ferrer and M. Calame, *In situ* Formation of One-Dimensional Coordination Polymers in Molecular Junctions, *Nat. Commun.*, 2019, **10**, 262.

21 K. Song, J. Lin, X. Song, M. Zhang, Q. Gu, Y. Zang and D. Zhu, In Situ Creation of Organometallic Molecular Junctions via Terminal Alkynes, *J. Phys. Chem. C*, 2023, **127**, 8850–8855.

22 X. Pan, B. Lawson, A. M. Rustad and M. Kamenetska, PH-Activated Single Molecule Conductance and, Binding Mechanism of Imidazole on Gold, *Nano Lett.*, 2020, **20**, 4687–4692.

23 A. Mishchenko, L. A. Zotti, D. Vonlanthen, M. Bürkle, F. Pauly, J. C. Cuevas, M. Mayor and T. Wandlowski, Single-Molecule Junctions Based on Nitrile-Terminated Biphenyls: A Promising New Anchoring Group, *J. Am. Chem. Soc.*, 2011, **133**, 184–187.

24 M. S. Hybertsen, L. Venkataraman, J. E. Klare, A. C. Whalley, M. L. Steigerwald and C. Nuckolls, Amine-Linked Single-Molecule Circuits: Systematic Trends across Molecular Families, *J. Phys.: Condens. Matter*, 2008, **20**, 374115.

25 M. Kamenetska, S. Y. Quek, A. C. Whalley, M. L. Steigerwald, H. J. Choi, S. G. Louie, C. Nuckolls, M. S. Hybertsen, J. B. Neaton and L. Venkataraman, Conductance and Geometry of Pyridine-Linked Single-Molecule Junctions, *J. Am. Chem. Soc.*, 2010, **132**, 6817–6821.

26 S. Li, H. Yu, X. Chen, A. A. Gewirth, J. S. Moore and C. M. Schroeder, Covalent Ag-C Bonding Contacts from Unprotected Terminal Acetylenes for Molecular Junctions, *Nano Lett.*, 2020, **20**, 5490–5495.

27 S. Li, Y. Jiang, Y. Wang and S. Hou, The Formation and Conducting Mechanism of Imidazole-Gold Molecular Junctions, *ChemistrySelect*, 2021, **6**, 2959–2965.

28 M. Liu, X. Han, H. Huang, X. Long and B. Tan, Controllable Sensitivity Mechanism in an Energetic Compound of [FeII(Rtrz)$_6$] as a Molecular Switch, *Chem. Phys. Lett.*, 2022, **801**, 139682.

29 O. Roubeau, Triazole-Based One-Dimensional Spin-Crossover Coordination Polymers, *Chem. – Eur. J.*, 2012, **18**, 15230–15244.

30 N. Wazzan, I. B. Obot and T. M. Fagieh, The Role of Some Triazoles on the Corrosion Inhibition of C1020 Steel and Copper in a Desalination Descaling Solution, *Desalination*, 2022, **527**, 115551.

31 W. Li, B. Tan, S. Zhang, L. Guo, J. Ji, M. Yan and R. Wang, Insights into Triazole Derivatives as Potential Corrosion

 

Inhibitors in CMP Process: Experimental Evaluation and Theoretical Analysis, *Appl. Surf. Sci.*, 2022, **602**, 154165.
32 Q. Wan, H.-Y. Guo, Y.-F. Zhou, J.-N. Jiang, W. Chen, J.-F. Zheng, Y. Shao, Y.-H. Wang and X.-S. Zhou, The Regulation Effect of Coordination Number on the Conductance of Single-Molecule Junctions, *J. Mater. Chem. C*, 2024, **12**, 60–65.
33 I. L. Herrer, A. K. Ismael, D. C. Milán, A. Vezzoli, S. Martín, A. González-Orive, I. Grace, C. Lambert, J. L. Serrano, R. J. Nichols and P. Cea, Unconventional Single-Molecule Conductance Behavior for a New Heterocyclic Anchoring Group: Pyrazolyl, *J. Phys. Chem. Lett.*, 2018, **9**, 5364–5372.
34 B. Schulze and U. S. Schubert, Beyond Click Chemistry-Supramolecular Interactions of 1,2,3-Triazoles, *Chem. Soc. Rev.*, 2014, **43**, 2522–2571.
35 S. Nasri, M. Bayat and K. Kochia, Strategies for Synthesis of 1,2,4-Triazole-Containing Scaffolds Using 3-Amino-1,2,4-Triazole, *Mol. Divers.*, 2022, **26**, 717–739.
36 G. Rauhut, Modulation of Reaction Barriers by Generating Reactive Intermediates: Double Proton Transfer Reactions, *Phys. Chem. Chem. Phys.*, 2003, **5**, 791–800.
37 J. A. Joule and K. Mills, *Heterocyclic Chemistry*, Wiley-Blackwell, 5th edn, 2010.
38 L. Venkataraman, J. E. Klare, I. W. Tam, C. Nuckolls, M. S. Hybertsen and M. L. Steigerwald, Single-Molecule Circuits with Well-Defined Molecular Conductance, *Nano Lett.*, 2006, **6**, 458–462.
39 J. McNeely, N. Miller, X. Pan, B. Lawson and M. Kamenetska, Angstrom-Scale Ruler Using Single Molecule Conductance Signatures, *J. Phys. Chem. C*, 2020, **124**, 13427–13433.
40 X. Pan, C. Qian, A. Chow, L. Wang and M. Kamenetska, Atomically Precise Binding Conformations of Adenine and Its Variants on Gold Using Single Molecule Conductance Signatures, *J. Chem. Phys.*, 2022, **157**, 234201.
41 X. Pan, E. Montes, W. Y. Rojas, B. Lawson, H. Vázquez and M. Kamenetska, Cooperative Self-Assembly of Dimer Junctions Driven by π Stacking Leads to Conductance Enhancement, *Nano Lett.*, 2023, **23**, 6937–6943.
42 L. A. Nagahara, T. Thundat and S. M. Lindsay, Preparation and Characterization of STM Tips for Electrochemical Studies, *Rev. Sci. Instrum.*, 1989, **60**, 3128–3130.
43 T. Fu, S. Smith, M. Camarasa-Gómez, X. Yu, J. Xue, C. Nuckolls, F. Evers, L. Venkataraman and S. Wei, Enhanced Coupling through π-Stacking in Imidazole-Based Molecular Junctions, *Chem. Sci.*, 2019, **10**, 9998–10002.
44 Z. Miao, T. Quainoo, T. M. Czyszczon-Burton, N. Rotthowe, J. M. Parr, Z.-F. Liu and M. S. Inkpen, Charge Transport Across Dynamic Covalent Chemical Bridges, *Nano Lett.*, 2022, **22**, 8331–8338.
45 L. Venkataraman, Y. S. Park, A. C. Whalley, C. Nuckolls, M. S. Hybertsen and M. L. Steigerwald, Electronics and Chemistry: Varying Single-Molecule Junction Conductance Using Chemical Substituents, *Nano Lett.*, 2007, **7**, 502–506.
46 A. Arnold, F. Weigend and F. Evers, Quantum Chemistry Calculations for Molecules Coupled to Reservoirs: Formalism, Implementation, and Application to Benzenedithiol, *J. Chem. Phys.*, 2007, **126**, 174101.
47 V. Blum, R. Gehrke, F. Hanke, P. Havu, V. Havu, X. Ren, K. Reuter and M. Scheffler, Ab Initio Molecular Simulations with Numeric Atom-Centered Orbitals, *Comput. Phys. Commun.*, 2009, **180**, 2175–2196.
48 J. Wilhelm, M. Walz, M. Stendel, A. Bagrets and F. Evers, Ab Initio Simulations of Scanning-Tunneling-Microscope Images with Embedding Techniques and Application to $C_{58}$-Dimers on Au(111), *Phys. Chem. Chem. Phys.*, 2013, **15**, 6684–6690.
49 J. P. Perdew, K. Burke and M. Ernzerhof, Generalized Gradient Approximation Made Simple, *Phys. Rev. Lett.*, 1996, **77**, 3865–3868.
50 B. Lawson, P. Zahl, M. S. Hybertsen and M. Kamenetska, Formation and Evolution of Metallocene Single-Molecule Circuits with Direct Gold- π Links, *J. Am. Chem. Soc.*, 2022, **144**, 6504–6515.
51 C. Toher, A. Filippetti, S. Sanvito and K. Burke, Self-Interaction Errors in Density-Functional Calculations of Electronic Transport, *Phys. Rev. Lett.*, 2005, **95**, 146402.
52 M. Koentopp, K. Burke and F. Evers, Zero-Bias Molecular Electronics: Exchange-Correlation Corrections to Landauer's Formula, *Phys. Rev. B: Condens. Matter Mater. Phys.*, 2006, **73**, 121403.
53 S.-H. Ke, H. U. Baranger and W. Yang, Role of the Exchange-Correlation Potential in Ab Initio Electron Transport Calculations, *J. Chem. Phys.*, 2007, **126**, 201102.
54 S. Y. Quek, L. Venkataraman, H. J. Choi, S. G. Louie, M. S. Hybertsen and J. B. Neaton, Amine - Gold Linked Single-Molecule Circuits: Experiment and Theory, *Nano Lett.*, 2007, **7**, 3477–3482.
55 F. Evers, R. Korytár, S. Tewari and J. M. Van Ruitenbeek, Advances and Challenges in Single-Molecule Electron Transport, *Rev. Mod. Phys.*, 2020, **92**, 035001.
56 S. Y. Quek, M. Kamenetska, M. L. Steigerwald, H. J. Choi, S. G. Louie, M. S. Hybertsen, J. B. Neaton and L. Venkataraman, Mechanically Controlled Binary Conductance Switching of a Single-Molecule Junction, *Nat. Nanotechnol.*, 2009, **4**, 230–234.